JMATPRO	Journal of Advanced Materials and Processing 10 (4): 13-24, Autumn 2022 http://jmatpro.iaun.iau.ir 20.1001.1.2322388.2022.10.4.2.1

Research Paper

Effects of Fe and Si Additions on Erosion-Oxidation Behavior of Nickel Alloys in Chlorine-Containing Oxidative Atmospheres

Mohammad Emami[1*], **Shigenari Hayashi**[2]

1. Assistant Professor, Department of Materials Science and Engineering, University of Bonab, Bonab, Iran.

2. Professor, Division of Materials Science and Engineering, Hokkaido University, Sapporo, Japan

ARTICLE INFO

Article history:

Received 30 June 2022
Accepted 6 August 2022
Available online 1 September 2022

Keywords:
High temperature erosion-oxidation
Fluidized bed
Nickel alloy
Fe effect
Si effect

ABSTRACT

High-temperature erosion-oxidation (E-O) of Ni-20Cr-(0-30)Fe-(0-4)Si was investigated in fluidized bed waste incineration conditions. The specimens were tested in a rig for 250 h, under the collision of hot silica sand contaminated with 0.5 wt.% of NaCl-KCl salt mixture at a temperature of 700 °C. To have a better understanding of the materials' behavior, the specimens were also oxidized at 560 °C for 100 h in the atmosphere of air + chlorine vapors. The thickness reduction and mass gain of the specimens were used to evaluate the materials under E-O and oxidation conditions, respectively. The specimens were studied using FESEM, EDS, and XRD analysis. At E-O conditions, Ni-20Cr showed the highest material loss (~17.6 μm). The addition of 30 wt.% of Fe to the alloy decreased the wastage to about 6.7 μm. The E-O resistance of Ni-20Cr-30Fe-4Si was about two times lower than the Si-free alloy which indicates that Si had a detrimental effect on the E-O resistance of the alloys. Under oxidation conditions, Ni-20Cr-30Fe showed the highest resistance with a mass gain of about 0.1 mg/cm^2. The addition of 4 wt.% Si caused a dramatic decrease in the oxidation resistance of the alloy (mass gain of ~3.8 mg/cm^2). The addition of Fe stimulated Cr_2O_3 scale formation by which the higher E-O and oxidation resistance of the alloy were confirmed. In Ni-20Cr, the formation of a multi-component scale, and in Ni-20Cr-30Fe-4Si, a porous surface scale formed through active oxidation were possibly responsible for the poor performance of these alloys.

Citation: Emami, M.; Hayashi, Sh. (2022). Effects of Fe and Si Additions on Erosion-Oxidation Behavior of Nickel Alloys in Chlorine-Containing Oxidative Atmospheres, Journal of Advanced Materials and Processing, 10 (4), 13-24. Dor: 20.1001.1.2322388.2022.10.4.2.1

[*] **Corresponding Author:**
E-Mail: memami@ubonab.ac.ir

1. Introduction

The emergence of new technologies such as using municipal waste to produce electricity has made more complex and aggressive environments develop compared to those of conventional fossil fuels [1]. Such environments contain low amounts of chlorine-bearing gases caused by burning polyvinyl chloride (PVC) in waste incinerators [2]. The presence of a mere several ppm of chlorine in a high-temperature oxidative atmosphere could significantly affect the oxidation kinetics [3]. In fluidized bed waste incinerators, the conditions are more complicated because hot sand particles that are used to increase the heating efficiency, remove the oxide scale formed on the surface of the boiler tubes continuously and cause severe material wastage through a complex process called high-temperature erosion-oxidation (E-O) [4]. Therefore, material selection and alloy development for such environments have become a subject of research in recent years [4-6]. The mechanisms of high-temperature E-O in oxidative atmospheres have been studied [7-9]. Different regimes of degradation including oxide erosion [7, 9], metal erosion [7, 9], oxidation-affected erosion [7, 9], and erosion-enhanced oxidation [8] have been widely accepted. The influence of the incidence angle of the eroding particles was evaluated. The specimens faced the maximum and minimum mass loss at an angle of 30° and 90°, respectively [10]. The high-temperature E-O of alloys has been studied in different aspects. The E-O behavior of SS316L and Inconel 740H at room temperature and 800°C was studied. At ambient temperature, SS316L showed higher erosion resistance. However, at 800°C, the hardness of SS316L reduced and the oxide scale was spalled off. Therefore, the E-O resistance of SS316L reduced significantly. Because Inconel 740H had higher mechanical properties at elevated temperatures, it outperformed stainless steel at 800 °C [11]. The E-O behavior of several Ni and Fe-based superalloys in an actual boiler environment was investigated. It was concluded that alloying elements especially chromium were the main factors affecting the alloys' degradation rate [12]. The E-O behavior of Superni-750 in a real coal-fired boiler was studied and it was suggested that a continuous chromia scale was important to guarantee the performance of the alloy [13]. The comparison of the E-O behavior of Ni and Fe alloys and superalloys showed that Cr addition was important in the materials' performance. It was also pointed out that conventional stainless steels performed better than more complicated superalloys. Such results directed the research toward developing much simpler alloy systems [14]. Nickel chlorides have rather high melting points and low vapor pressures that favor nickel as a base material for chlorine-bearing atmospheres [15].

In general, the behavior of an alloying element in an oxidizing atmosphere does not necessarily replicate that in an oxidizing-chloridizing atmosphere. This is because some elements such as chromium form volatile chlorides/oxychlorides, but their oxides are highly stable [15]. Under severe conditions of E-O where the corrosion product is partially removed by colliding particles, the situation is more complicated. In pursuit of implementing new alloy systems with fewer alloying elements to resist high-temperature erosion-corrosion in fluidized bed waste incineration, it is vital to figure out such interrelations between the alloying elements content, corrosive media, and mechanical degradation by the erosion. The effect of Mo on the high-temperature E-O of Ni-20Cr alloys was studied in earlier research. It was found that higher contents of Mo had detrimental effects on the alloy performance [16]. The E-O rate increased by repeated erosion of a Ni-rich oxide layer and spallation of the oxide scale. The spallation was attributed to the formation of an inner porous scale caused by the volatilization of Mo oxychloride [5]. The study of the Si additions to the same alloy system showed that Si-enhanced Cr diffusion in the alloy reduced the Cr-depleted zone and consequently eliminated internal oxidation. However, Si caused the spallation of the oxide scale and its rapid removal by the impacting particles [17].

Fe is usually known as an element to improve the economy of Ni alloys [18]. However, the role of Fe in the high-temperature E-O of the Ni-20Cr alloys is not clear. This paper aims to evaluate the effects of Fe and Fe in combination with Si on the erosion-oxidation behavior of Ni-20Cr model alloys in fluidized bed waste incineration conditions.

2. Materials and methods

based-Nickel alloys with dimensions of 20×10×1 mm^3 and the nominal compositions shown in Table 1 were prepared in a vacuum arc remelting furnace under a vacuum level of 2×10^{-5} torr followed by 48 h of normalizing process in a vacuum tube furnace at 1200 °C. The optical micrographs of the alloys 30Fe and 30Fe-4Si after normalizing could be seen in Fig. 1 which show single-phase microstructures.

Table 1. Nominal chemical composition of the alloys (wt.%)

Sample	Ni	Cr	Fe	Si
0Fe	80	20	-	-
10Fe	70	20	10	-
30Fe	50	20	30	-
30Fe-2Si	48	20	30	2
30Fe-4Si	46	20	30	4

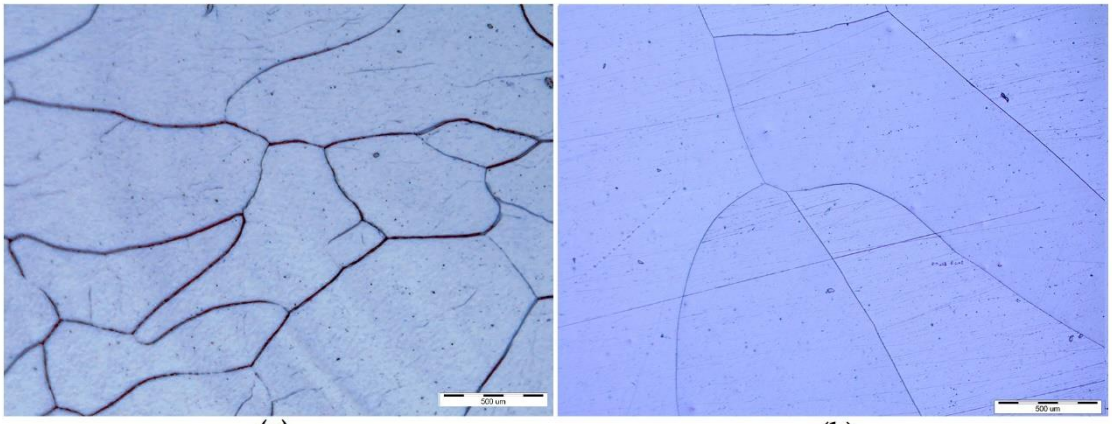

(a) **(b)**

Fig. 1. Optical micrographs of the alloys 30Fe and 30Fe-4Si after 48 h of normalizing at 1200°C.

The specimens were tested in a rig, schematically shown in Fig. 2, which was designed and customized for the evaluation of the E-O behavior of alloys in fluidized bed waste incineration conditions. SiO_2 sand with a temperature of 700 °C, contaminated with 0.5 wt.% of equimolar NaCl/KCl mixture, was used as the erodent. The sand was placed in a quartz reaction chamber. There was a quartz filter at the bottom of the chamber to let the air move in the chamber. The samples were pinned at an angle of 45° to the bottom of a cylindrical sample holder facing down to the eroding particles. Compressed air with a flow rate of 25 L/min was primarily heated by heater 1 at the air inlet. It was further heated to 400 °C passing through the quartz tube by heater 2 and caused the sand to move and make a fluidized bed of particles collide with the specimens for 250 h. A crucible of salt was placed below and outside the reaction chamber at 550 °C to ensure a continuous supply of salt vapor to the environment. To evaluate the E-O resistance of the alloys, the thickness reduction of the specimens was measured. For this purpose, a laser thickness measurement device based on the mechanism of light reflection from a constant point with a precision of 0.1 μm was used. For more accuracy, the thickness of eight equidistant points on the middle line of the specimens was measured before and after the experiments and the mean value was reported. To have a better understanding of the behavior of the alloys in erosive conditions, a set of oxidation experiments was performed at 560 °C for 100 h in an atmosphere of air containing small amounts of NaCl-KCl-$CaCl_2$ salt vapor. For this purpose, a crucible of a salt mixture (KCl-40 mol.% NaCl-20 mol.% $CaCl_2$) with a melting temperature of 517 °C was placed in the hot zone of a tube furnace next to the specimen. The chlorine potential of the atmosphere was calculated to be 3.7×10^{-6} atm [19]. To ensure steady-state conditions, a stream of air with a linear flow rate of 1 mm/s was blown in the furnace [20]. The oxidation temperature of 560 °C was chosen after numerous experiments at 450-700 °C for evaluating the scaling behavior of the alloys in comparison with E-O experiments. For the evaluation of the oxidation resistance of the alloys, the mass change after 100 h of oxidation was measured using a balance with a precision of 10-6 g. For each alloy, three specimens were tested and the mean value of the mass change was reported. The surface and cross-section of the samples were observed using field emission scanning electron microscopy (FESEM) equipped with energy dispersive X-ray spectroscopy (EDS). Since the oxide scales were thin, the preparation of the cross-sections was carried out by focused ion beam (FIB) using gallium ion, through several rough and fine milling steps. A FIB-FESEM JIB-4700F multi-beam system was used for preparation and observation purposes. X-ray diffractometry was performed to characterize surface layers. For thicker scales XRD was carried out in the normal mode using Cu-kα radiation, $20° < 2\theta < 80°$, step size of 0.04 in 40 kV and 30 mA. For thinner scales, a low-angle technique at 5° at three 2Θ ranges of 20-40°, 40-60°, and 60-80° was utilized.

3. Results and discussion

3.1 Erosion-corrosion behavior of the alloys

In high temperature erosion-corrosion, the material is lost by a persistent oxidation and wear process [12]. Therefore, the thickness of the material is reduced during the process. So, the thickness reduction of the materials was taken as the measure for the E-O resistance of the alloys. The thickness reduction of different alloys after 250 h of E-O is shown in Fig. 3. It is noted that when the iron content of the alloys increased from 0 wt.% to 30 wt.%, the E-O resistance of the alloy increased by about 3 times. However, adding 2 and 4 wt.% of Si to Ni-20Cr-30Fe alloy with the highest E-O resistance led to an increased thickness reduction of the alloy to as low as that of 10Fe alloy which shows the detrimental effect of Si on the E-O resistance of the alloys.

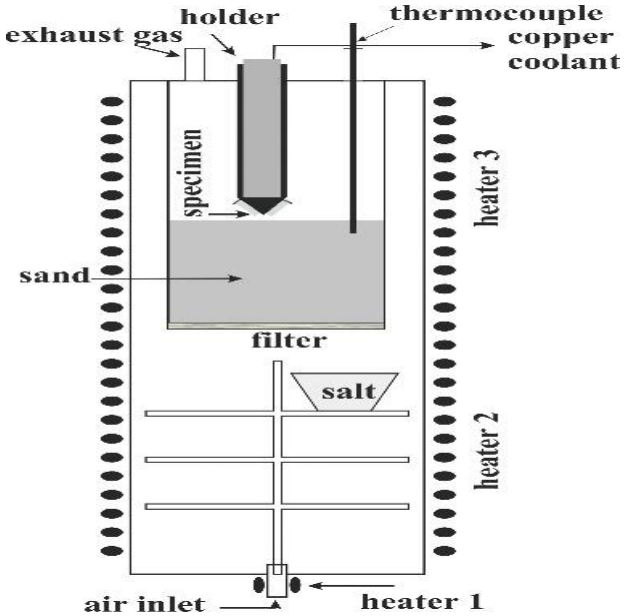

Fig. 2. Schamatic representaion of the E-O test rig.

In order to identify the oxide scales that remained on the alloy surfaces after 250 h of E-O, XRD patterns were obtained for samples 0Fe, 10Fe, and 30Fe (Fig. 4). Because the remained oxide scale was not thick enough, no reliable data was attained for Si-containing alloys. The results show the formation of NiO and Ni-Cr spinel ($NiCr_2O_4$) on the surface of alloys 0Fe and 10Fe. In the case of alloy 30Fe, chromia and spinel appear to be dominant reaction products. This could imply that the addition of 30 wt.% Fe to the base alloy affected the reaction products. In the XRD patterns, the Ni peaks come from the base alloy.

The SEM micrographs of the eroded surface of samples 0Fe, 30Fe, and 30Fe-4Si are shown in Fig. 5. The surface of all samples is covered with a thin oxide layer. Because of the impact of sand particles on the surface, some scratches and craters appeared. However, in the case of sample 30Fe-4Si (Fig. 5c) the damage is apparently more intense which is in agreement with the thickness reduction results. The SEM micrographs of the cross-section of the samples 0Fe, 30Fe, and 30Fe-4Si after 250 h of E-O under the test conditions are illustrated in Fig. 6. An uneven surface covered with a thin layer of oxide is noted in all alloys. The thickness of the oxide layer was about 130 nm, 280 nm, and 136 nm in the case of 0Fe, 30Fe, and 30Fe-4Si, respectively. It means that the oxide layer remained on 30Fe with the highest E-O resistance is twice as thick as the other two alloys. Studies on the E-O behavior of Ni-20Cr-4Fe alloy showed an oxide scale thickness of about 80 nm and 320 nm after 50 h and 250 h, respectively. The addition of 7 wt.% of Mo to the above alloy caused a complete removal of the oxide scale after 250 h [5]. Moreover, in the case of alloy 30Fe-4Si, the oxide scale is seemingly more interrupted as a result of the severe erosive attack observed in Fig. 6c.

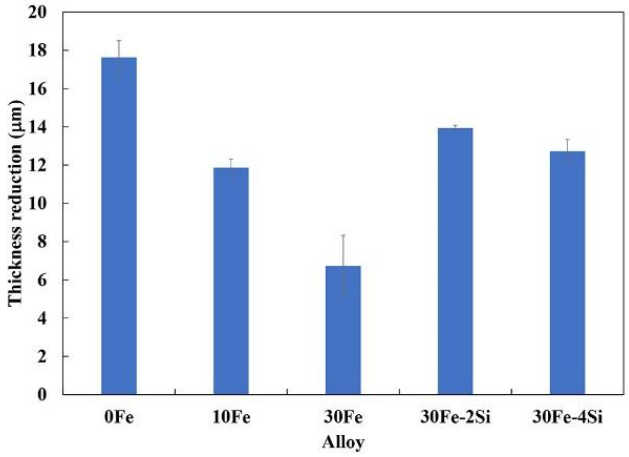

Fig. 3. Thickness reduction of different alloys after 250 h of E-O.

The EDS elemental analysis of different areas shown in Fig. 6 is tabulated in Table 2. It should be noted that EDS analysis is a semi-quantitative method. Also, the oxide scales in the present study are thinner than the electron spot size, and getting some signals from the base alloy is unavoidable. So, the chemical compositions in Table 2 are partly decisive. Analysis of point 1 shows Ni, Cr, and O in the oxide which shows oxide formation. However, this analysis does not give trustworthy information about the oxide's composition. According to Table 2 and Fig. 6a, a Cr-depleted zone with a depth of about 600 nm was formed in sample 0Fe which shows the intensive consumption of Cr in this alloy in the form of a spinel phase. Regarding alloy 30Fe, the depth of Cr depletion was reduced to one-fifth of that in 0Fe (~120 nm). The depletion of Fe in this alloy could be attributed to the incorporation of Fe in the oxidation products like $(Cr, Fe)_2O_3$ which is likely to form despite different defect structures of Cr_2O_3 and Fe_2O_3 [21]. Even though Cr depletion in 0Fe and 30Fe was evident, one could not find internal oxides in the near-surface depleted regions. Regarding alloy 30Fe-4Si, analysis of point 8 in Fig. 6c confirmed no tangible depletion of Cr or Fe.

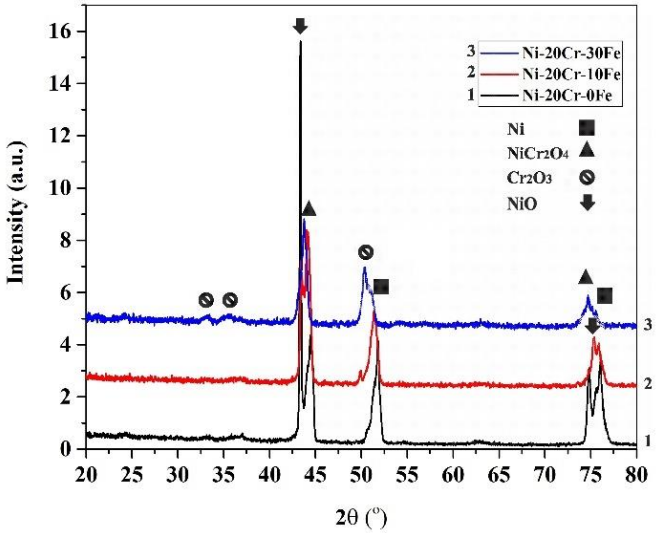

Fig. 4. XRD patterns of the surface of alloys 0Fe, 10Fe, and 30Fe after 250 h of E-O.
JCPDS cards: Ni (#04-0850), NiO (#44-1159), $NiCr_2O_4$ (#23-0432), Cr_2O_3 (#38-1479).

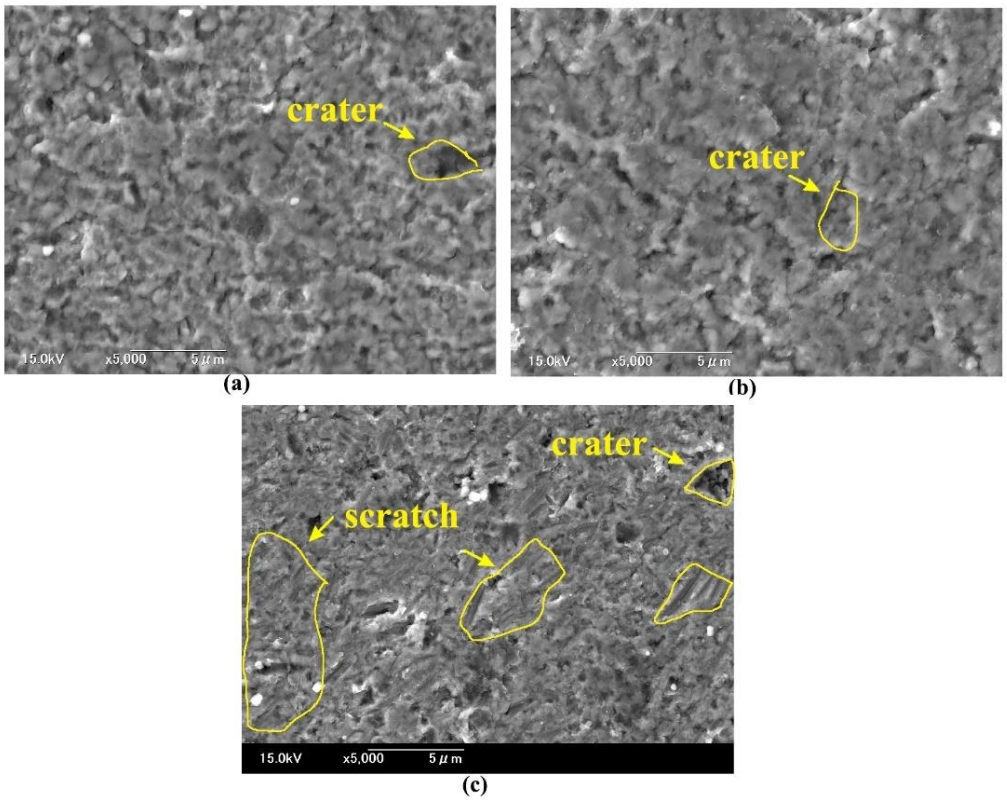

Fig. 5. SEM micrographs of the surface of alloys 0Fe, 30Fe, and 30Fe-4Si after 250 h of E-C.

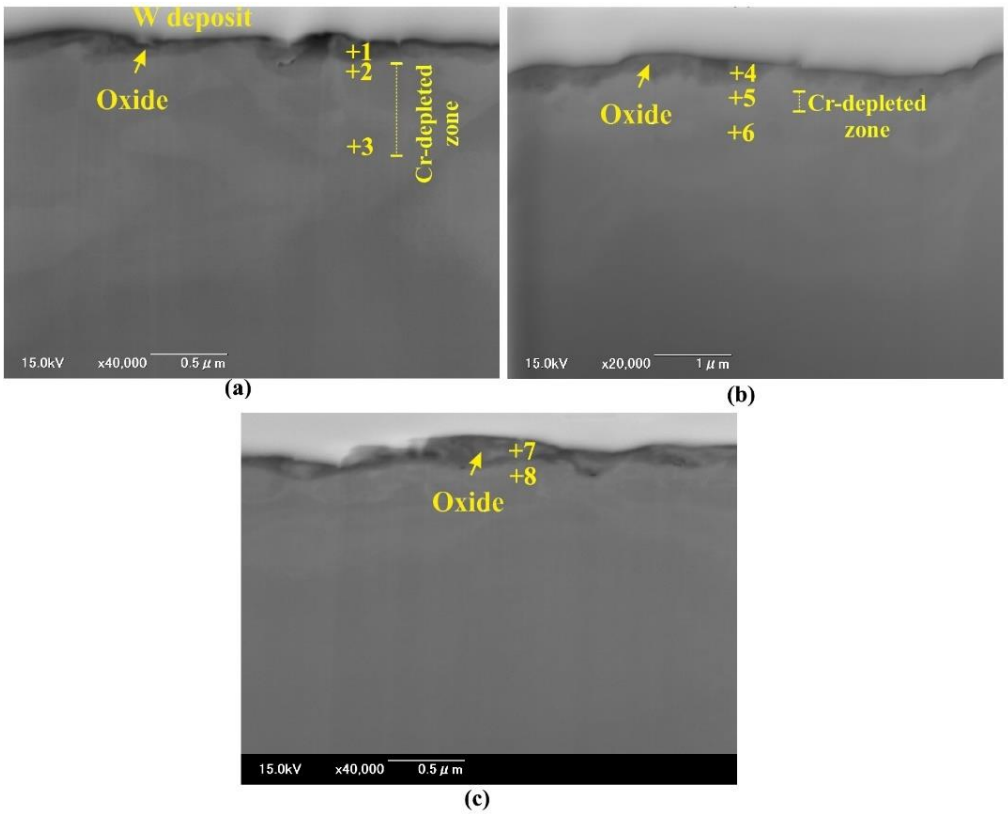

Fig. 6. SEM micrographs of the cross-sections of alloys 0Fe, 30Fe, and 30Fe-4Si after 250 h of E-C.

Table 2. EDS elemental analysis of different points on Fig. 6 and Fig.9 (at.%)

	Ni	Cr	Fe	Si	O	Cl	Ca	K	Na
1	56.3	31.7	-	-	11.7	-	-	0.2	-
2	87.3	11	-	-	1.4	0.2	-	-	-
3	82.1	17.7	-	-	-	0.2	-	-	-
4	40.3	22.3	26.3	-	10.7	0.3	0.2	-	-
5	59	16.2	21.3	-	1	1.3	0.6	-	0.5
6	29.1	22.1	28.8	-	-	-	-	-	-
7	40.9	18.1	26.5	8.1	6.1	-	-	0.2	-
8	42.6	21.8	29.4	6.2	-	-	-	-	-
9	74.8	5	-	-	20	0.1	-	-	-
10	43	25.2	-	-	22.7	0.1	0.1	8.4	0.6
11	39	38.3	-	-	22.4	0.1	0.1	0.2	-
12	32.3	52.2	-	-	15	0.4	-	-	-
13	77.3	22.4	-	-	0.1	0.2	0.2	-	-
14	17	42.1	22.2	-	18.1	0.3	0.2	-	-
15	45	28.7	24	-	2.1	0.1	0.1	0.1	-
16	22.8	22	25.2	4.3	24.9	0.3	0.4	0.2	-
17	42.9	24	27.1	3.5	1.5	0.5	0.3	0.1	-

3.2. Oxidation of the alloys in flowing air containing chlorine vapor

Since high-temperature E-O is a complex interaction of high-temperature oxidation and removal of surface scales by hard particles, it has been established that for a better understanding of the E-O behavior of an alloy, its oxidation behavior ought to be known, too [9]. The mass gain results of different samples after 100 h of oxidation in air + chlorine vapors at 560 °C are presented in Fig. 7. Alloy 30Fe showed the lowest corrosion rate (~0.04 mg/cm^2). Reducing the Fe content of the alloys to 10 and 0 wt.% led to an increase in the alloy oxidation rate to about 4 and 13 times, respectively. It appears that Fe has an exceptionally positive effect on the oxidation resistance of Ni-20Cr alloys under test conditions. However, the addition of 4 wt.% of Si deteriorated the oxidation resistance and caused the oxidation rate of 30Fe-4Si to increase 9 orders of magnitude compared to that of 30Fe.

Regarding XRD results in Fig. 8a, alloy 0Fe shows a complex oxide scale comprising NiO, Cr_2O_3, and $NiCr_2O_4$ together with a non-protective potassium dichromate compound ($K_2Cr_2O_7$). The latter forms through the reaction of vapors of KCl with the chromia scale through equation (1), and acts as a sink for Cr [22] which leads to the breakdown of the protective scale [23-25].

$$2KCl(g) + Cr_2O_3(s) + 2O_2(g) = K_2Cr_2O_7(s) + Cl_2(g) \quad (1)$$

The oxidation products in alloy 10Fe were more or less similar to those of 0Fe. However, the oxide scale on alloy 30Fe mostly comprised Cr_2O_3/$(Cr, Fe)_2O_3$. As in the case of the E-O experiments of alloy 30Fe, it could be argued that the addition of 30 wt.% Fe to a Ni-20Cr alloy stabilized Cr_2O_3. Silicon-containing alloys showed a different oxide scale with the composition of $(Fe, Ni)Cr_2O_4$ (Fig. 8b) which is a spinel of Fe, Ni, and Cr. The study of the oxidation behavior of Ni-20Cr alloy in the air at 570 °C showed that a chromium oxide scale and some oxides growing toward the inner areas of the alloy were formed. When the alloy was tested at air + chlorine, some deposits of NaCl appeared on the oxide scale. Also, KCl caused a potassium chromate layer to form on the surface which was responsible for the breakdown in the protection of the oxide scale [19]. This shows that even small amounts of chlorine vapors affected the oxidation behavior and protectiveness of the oxide scales.

The SEM micrographs of the cross-section of alloy 0Fe after 100 h of oxidation could be seen in Fig. 9a. A mixed oxide scale with a thickness of about 1.7 μm is observed. The chemical composition of points 9, 10, 11, and 12 in Table 2 agrees with the XRD results (Fig. 8). At point 12 the chlorine content of 0.4 at.% at the interface between the oxide scale and the base material implies a chlorine attack on the material. The chlorine attack is widely accepted to happen through the formation of molecular chlorine on the surface and its diffusion through pores and cracks on the oxide [1, 22]. There are also some voids at the interface that might be associated with the formation of volatile chlorides/ oxychlorides. The analysis of the near-surface area (point 13) showed no Cr depletion in this alloy. The thickness of the oxide scale of alloy 30Fe with the highest oxidation resistance was about 250 nm i.e. about 7 times lower than that of alloy 0Fe (Fig. 9b). The oxide scale in this alloy is perhaps $(Cr, Fe)_2O_3$, as discussed earlier

in the E-O results of the same alloy. The oxide scale on alloy 30Fe-4Si with a thickness of about 4.2 μm shows totally different characteristics. Such a porous scale is indicative of the formation of volatile chloride compounds which promotes accelerated active oxidation [1]. The EDS analysis of the subsurface area of alloys 30Fe and 30Fe-4Si showed no signs of Cr-depletion. However, some signals of Cl in points 15 and 17 may indicate the diffusion of Cl into the alloy.

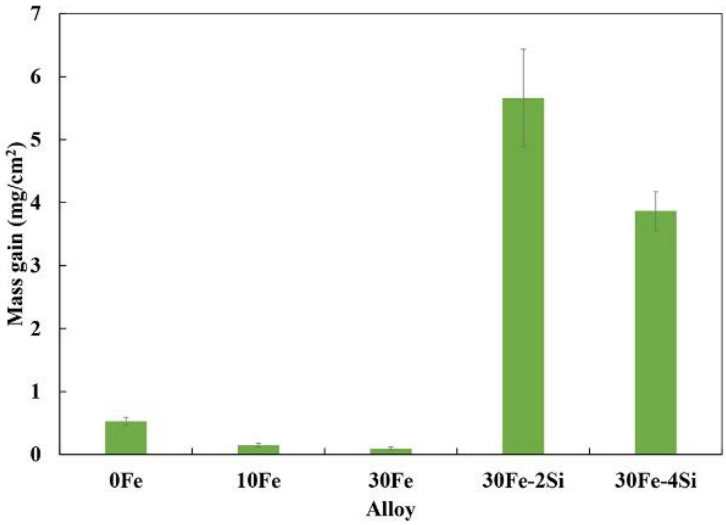

Fig. 7. Mass gain of the alloys after 100 h of oxidation at 560 °C in air + chlorine vapors.

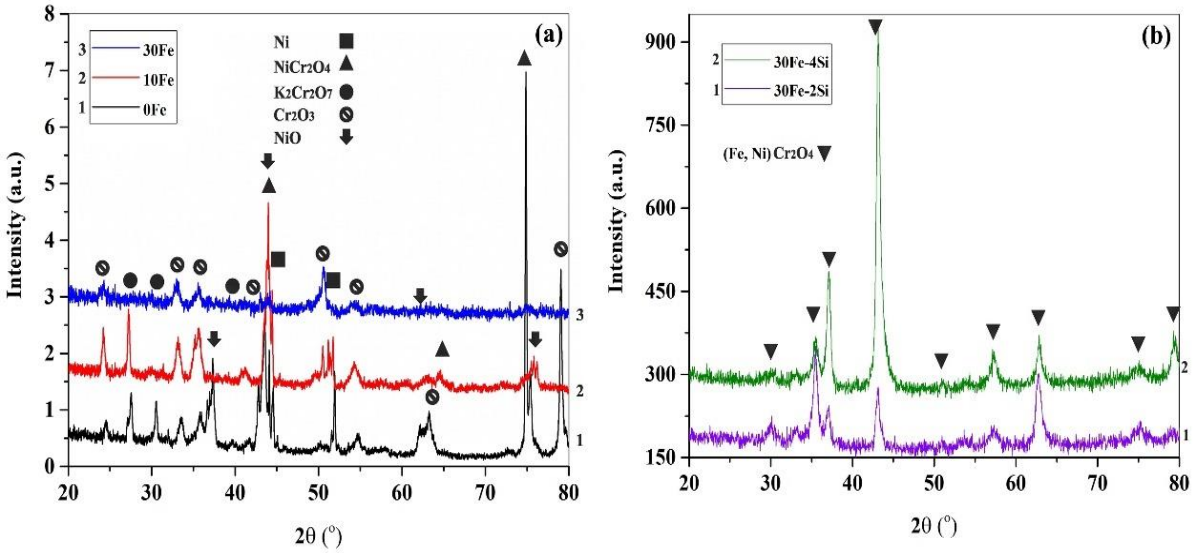

Fig. 8. XRD patterns of the surface of the alloys after 100 h of oxidation at 560°C in air + chlorine vapors.
(a) 0Fe, 10 Fe, and 30Fe, (b) 30Fe-2Si and 30Fe-4Si. Note: JCPDS cards: Ni (#04-0850), NiO (#44-1159), $NiCr_2O_4$ (#23-0432), Cr_2O_3 (#38-1479), $K_2Cr_2O_7$ (#00-001-0676).

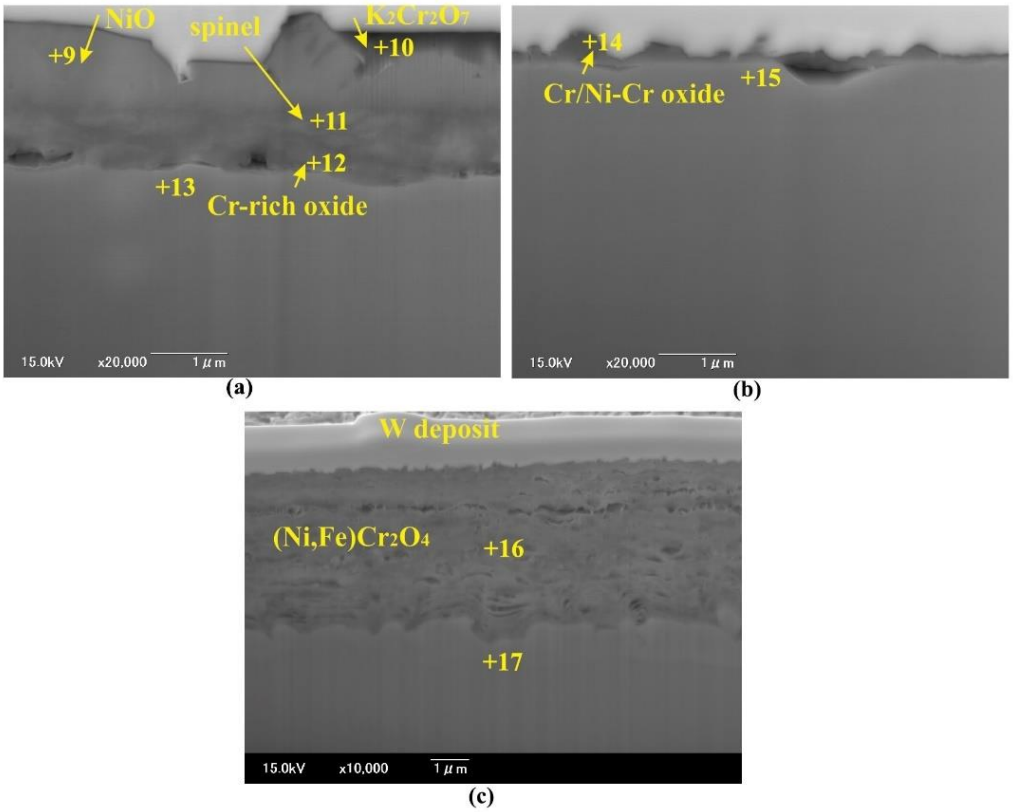

Fig. 9. SEM micrographs of the cross-sections of alloys 0Fe, 30Fe, and 30Fe-4Si after 100 h of oxidation at 560 °C in air + chlorine vapors.

In the case of alloys 0Fe and 10Fe, after 100 h of oxidation in air + chlorine vapors at 560 °C a multicomponent oxide scale formed consisting of more protective Cr_2O_3 and $NiCr_2O_4$ and less protective NiO oxides. This in turn could expose the oxide to further mechanical damage by developing internal stresses caused by varying thermal expansion coefficients of 17.1×10^{-6} K^{-1}, 8.5×10^{-6} K^{-1}, and 17.6×10^{-6} K^{-1} for NiO, Cr_2O_3, and Ni, respectively [26]. Oxidation of the alloy starts with a transition stage in which NiO forms before a chromia scale is stabilized. The extent of this transient stage depends on the conditions that promote the selective oxidation of chromium. In the case of Ni-20Cr alloy and the oxidation conditions in this study, it seems that Cr content was not enough for a continuous chromia scale to be established. According to Wagner's theory, the minimum Cr content is obtained using the following equation (2):

$$N_{Cr}^{(o)} \geq \left[\frac{\pi g^*}{2\nu} N_O^{(s)} \frac{D_O V_m}{D_{Cr} V_{ox}}\right]^{1/2} \quad (2)$$

where $N_{Cr}^{(o)}$ is the initial Cr content in the alloy, g^* is the critical volume fraction of oxide for the transition from internal to external oxide, $N_O^{(s)}$ is the molar fraction of oxygen dissolved in the surface, D_O and D_{Cr} are the diffusivities of O and Cr, respectively, and V_m and V_{ox} are molar volumes of the solvent metal and CrO_v, respectively. To measure $N_{Cr}^{(o)}$ for the current case, g^* is considered as 0.3 [1, 27], ν is 1.5 for Cr_2O_3, V_m and V_{ox} are 6.7 and 14.56 cm^3/mole, respectively. The data in [28] and [29] were used to approximate D_O and D_{Cr}. $N_O^{(s)}$ could be obtained by Equation (3), where $\underline{O}$ denotes the dissolved oxygen in the alloy.

$$\frac{1}{2} O_2(g) = \underline{O} \quad (3)$$

For this reaction, $\Delta G = \Delta G^{XS} + \Delta G^{M,id}$. So,

$$\Delta G = \Delta \bar{H}_O - T\Delta \bar{S}_O^{XS} + RTlnN_O - \frac{1}{2}RTlnP_{O_2} \quad (4)$$

If $\Delta \bar{H}_O$= -182 $kJmol^{-1}$ and $\Delta \bar{S}_O^{XS}$= -107.6 $Jmol^{-1}K^{-1}$ [1] and the maximum solubility of oxygen in nickel is calculated by the equilibrium between Ni and NiO, P_{O_2} and subsequently $N_O^{(s)}$ could be calculated at any given temperature. Therefore, at 560 and 700 °C, $N_{Cr}^{(o)}$ values of about 0.4 and 0.35 were obtained which is higher than the Cr content of the alloy in this study. Despite this, some factors like grain boundary or dislocation-assisted diffusion that accelerates the Cr diffusion in the alloy could lower the above values. Thus, it could be argued that 20 wt.% of Cr did not suffice for a single chromia layer formation and it was experimentally confirmed in Fig. 8a and Fig. 9a. Such a result was reported in the case of Ni-

20Cr alloy in wet CO_2 gas at 650 and 700 °C [27]. The spinel phase could form through a solid state reaction shown in Equation (5).

$$NiO + Cr_2O_3 = NiCr_2O_4 \quad (5)$$

The addition of 30 wt.% of Fe to the Ni-20Cr possibly shortened the transition oxidation and caused a continuous chromia scale form. It was suggested that iron could reduce the activation energy for the diffusion of Cr in Ni, from 283 kJ/mol in Ni-19.9%Cr to 277 kJ/mol in Inconel 600, because of a decrease in bond energy [30]. Similarly, in the present study, Fe might enhance the Cr outward diffusion and accelerate chromia formation.

The literature survey shows that Si could stimulate the formation a chromia scale [31] because its addition to the alloy could accelerate the Cr diffusion rate in the alloy. In the case of NiCr and NiCrFe alloys, it was reported that at 1000 °C, Si increased the Cr diffusion in Ni by 10 times [32]. However, it is emphasized that in many Si-containing alloys, Si may not perform well, because it may form highly volatile silicon tetrachloride at the interface between the alloy and oxide scale (where the oxygen partial pressure is too low), weakens the bonding between the scale and alloy, and prevents an already damaged oxide scale from healing up [31]. However, it has been thermodynamically confirmed that at high oxygen pressures and low chlorine pressure in this study, only oxides are stable [19]. Fig. 9c shows a porous oxide formed through the active oxidation mechanism. In this mechanism, the oxide formed on the surface could react with the chlorine that penetrated the oxide scale through pores and cracks to form the chloride of the metal [33]. Since chlorides have high vapor pressures, move upward through the scale. At higher oxygen partial pressures i.e. near the outer surface of the oxide scale, the chloride is thermodynamically unstable and transforms to oxide again. This oxide is otherwise porous and therefore could not protect the alloy from further oxidation. It was reported that the transformation of $SiCl_4$ to SiO_2 is kinetically too slow [31]. Thus, it seems that Si takes part in the material wastage in the form of vapor $SiCl_4$ rather than the mass gain. This could explain the higher mass gain of the alloy 30Fe-2Si. However, still Cr and Fe chlorides could actively take part in the active oxidation process.

Regarding E-O experiments, alloy 30Fe with the highest oxidation resistance had the best performance in erosive conditions. 0Fe and 30Fe-4Si which showed lower oxidation resistance, underperformed in E-O conditions, too. In high-temperature E-O, the oxide scale formed on the surface is partially removed by the impact of hard particles. So, the rate of E-O is expressed as the difference between the scale formation by oxidation and its removal by erosion. Concerning alloy 0Fe, a thick fast growing oxide scale formed during oxidation. However, a very thin scale remained on the surface after 250 h of E-O (Figs. 9a and 6a). This indicates that in this alloy, the oxide removal has exceeded its growth by oxidation. Since both oxidation and removal rates are fast, the alloy shows high wastage. The high erosion rate is associated with the mixed oxide and the subsequent internal stresses and also the non-protective and poorly adherent chromate phase. As was stated earlier, the chromate phase consumes lots of chromium without participating in the protectiveness of the oxide scale. This could explain Cr depletion in the subsurface regions of alloy 0Fe (Fig. 6a and Table 2). However, it is not clear why internal oxides are absent in the depleted areas.

In the case of alloy 30Fe-4Si, the damage mechanism is quite straightforward. The porous and layered oxide formed on the surface is not resistant to erosion. The impacting particles could simply remove the oxide scale and expose the material to accelerated oxidation and erosion. This is justified by the fact that in diffusion-controlled oxidation, the oxide scale initially grows rapidly. After it reaches a certain thickness, the diffusion of cations or anions in the scale slows down and oxidation proceeds at a steady state rate. When the oxide is removed rapidly, as in the case of the present study, the diffusion-controlled steady-state is not achieved and the oxidation continues rapidly. Therefore, the interaction of a fast-growing, non-protective, loose oxide and collision of hard particles leads to a high wastage rate of the alloy. The absence of the Cr-depleted zone in this alloy is attributed to the role of Si in increasing the Cr diffusion in the Ni substrate [32]. Therefore, Cr diffuses more rapidly from the internal zones to the subsurface areas compared to other alloys.

Alloy 30Fe showed the best performance in both oxidation and E-O conditions. It was suggested that maybe Fe promoted chromia formation. Chromia is a slow growing oxide that provides the alloy with excellent oxidation resistance. Such a thin and single phase oxide scale develops lower levels of stress in the scale. Besides, chromia has superior mechanical properties over NiO [34] and therefore is more mechanically resistant against eroding particles. Incorporation of Fe in the crystal structure of chromia in the form of $(Cr, Fe)_2O_3$ may incraese the toughness of the oxide and futher enhance the mechanical properties of the oxide.

4. Conclusions

The high-temperature erosion-oxidation under fluidized bed waste incineration and oxidation in air + chlorine vapors behaviors of Ni-20Cr alloys with various amounts of Fe (0-30wt.%) and Si (0-4wt.%) were investigated.

1- The alloy containing 30 wt.% Fe showed the highest E-O resistance with a wastage rate of about 6.7 μm/250 h. The SEM observations and XRD analysis showed a scale comprising Cr_2O_3 and $NiCr_2O_4$ with a thickness of about 280 nm. This alloy showed the highest oxidation resistance with a mass change of about 0.1 mg/cm^2. A protective $(Cr, Fe)_2O_3$ scale formed on the surface which was responsible for the alloy's performance in the corrosive atmosphere. Fe was suggested to accelerate the Cr diffusion and the formation of external chromium oxide and the resulting high-temperature E-O and oxidation resistance of the alloy.

2- In Ni-20Cr alloy, a scale comprising NiO, Cr_2O_3, $NiCr_2O_4$, and $K_2Cr_2O_7$ (thickness of ~ 1.7 μm) formed after 100 h of oxidation at 560 °C. 20 wt.% of Cr was considered insufficient to guarantee a protective chromia scale on the alloy surface. Such a multicomponent scale with different coefficients of thermal expansion was known to develop internal stresses in the oxide. Thus, the oxide was more prone to breakdown at the collision of eroding particles.

3- Si deteriorated the resistance of Ni-20Cr-30Fe alloy in both oxidation and E-O conditions. A porous, layered thick oxide (~4.2 μm) with the composition of $(Ni,Fe)Cr_2O_4$ formed after 100 h of oxidation in air + chlorine. Such a porous scale was not resistant to erosive conditions and was easily removed by impacting solid particles. The morphology of the oxide scale suggested the active oxidation mechanism that does not protect against oxidation. The formation of volatile silicon chlorides was probably responsible for interrupting the formation of a compact protective scale. However, Si led to an accelerated Cr diffusion in the alloy and the annihilation of the internal oxidation.

.

References

[1] D.J. Young, High temperature oxidation and corrosion of metals, 2 ed., Elsevier, 2015,

[2] A. Zahs, M. Spiegel, H.J. Grabke, "Chloridation and oxidation of iron, chromium, nickel and their alloys in chloridizing and oxidizing atmospheres at 400–700 °C", Corros. Sci., Vol. 42, No. 6, 2000, pp. 1093-1122.

[3] P. Hou, Y. Niu, T. Sum, J. Stringer, "Effect of HCl on the corrosion and wear of in-bed tubes in a laboratory simulated bubbling fluidized bed", Wear, Vol. 233, No. 1999, pp. 635-646.

[4] M. Noguchi, H. Yakuwa, M. Miyasaka, H. Sakamoto, S. Kosugi, T. Narita, "High temperature erosion-corrosion behavior of boiler tube materials in fluidized-bed waste incinerator conditions", Proc. Proceedings of High Temperature Corrosion and Protection 2000, pp. 573-578.

[5] S. Yoneda, S. Hayashi, Y. Miyakoshi, T. Kogin, E. Ishikawa, M. Noguchi, "Erosion-corrosion behavior of Ni-20Cr-4Fe and ni-20Cr-4Fe-7Mo under fluidized-bed biomass boiler conditions", Corros. Sci., Vol. 205, No. 2022, pp. 110472.

[6] R. Norling, I. Olefjord, "Erosion–corrosion of Fe- and Ni-based alloys at 550° C", Wear, Vol. 254, No. 1-2, 2003, pp. 173-184.

[7] C. Kang, F. Pettit, N. Birks, "Mechanisms in the simultaneous erosion-oxidation attack of nickel and cobalt at high temperature", Metallurgical Transactions A, Vol. 18, No. 10, 1987, pp. 1785-1803.

[8] S. Chang, F. Pettit, N. Birks, "Interaction between erosion and high-temperature corrosion of metals: The erosion-affected oxidation regime", Oxid. Met., Vol. 34, No. 1, 1990, pp. 23-45.

[9] R. Wellman, J. Nicholls, "High temperature erosion–oxidation mechanisms, maps and models", Wear, Vol. 256, No. 9-10, 2004, pp. 907-917.

[10] W. Wu, B. Wei, G. Li, L. Chen, J. Wang, J. Ma, "Study on ammonia gas high temperature corrosion coupled erosion wear characteristics of circulating fluidized bed boiler", Engineering Failure Analysis, Vol. 132, No. 2022, pp. 105896.

[11] E. Gietzen, S. Karimi, N. Goel, S.A. Shirazi, M. Keller, T. Otanicar, "Experimental investigation of low velocity and high temperature solid particle impact erosion wear", Wear, Vol. 506, No. 2022, pp. 204441.

[12] S.B. Mishra, K. Chandra, S. Prakash, "Erosion–corrosion behaviour of nickel and iron based superalloys in boiler environment", Oxid. Met., Vol. 83, No. 1, 2015, pp. 101-117.

[13] T. Sidhu, S. Prakash, R. Agrawal, R. Bhagat, "Erosion-corrosion behaviour of Ni-based superalloy superni-75 in the real service environment of the boiler", Sadhana, Vol. 34, No. 2, 2009, pp. 299-307.

[14] J. Tylczak, "Erosion–corrosion of iron and nickel alloys at elevated temperature in a combustion gas environment", Wear, Vol. 302, No. 2013, pp. 1633-1641.

[15] G. Y. Lai, High-temperature corrosion and materials applications, ed., ASM International, 2007,

[16] M. Emami, S. Hayashi, "High temperature erosion- oxidation behavior of nickel- based alloys containing Mo in fluidized bed waste incineration", iut-jame, Vol. 39, No. 3, 2020, pp. 41-54. (in Persian)

[17] M. Emami, S. Hayashi, "Effects of silicon on high temperature oxidation and erosion-oxidation behaviors of nickel alloys ", Journal of Corrosion Sciences and Engineering, Vol. 24, No. 2020, pp. 7-19. (in Persian)

[18] J.R. Davis, Alloying: Understanding the basics, ed., ASM international, 2001,

[19] H. Izzuddin, S. Hayashi, S. Yoneda, T. Kogin, E. Ishikawa, M. Noguchi, "Effect of Mo on corrosion

behavior of Ni20Cr–xMo alloys in air with NaCl–KCl–CaCl2 vapor at 570° c", Materials and Corrosion, Vol. 71, No. 9, 2020, pp. 1488-1499.
[20] T. Gheno, B. Gleeson, "On the hot corrosion of nickel at 700 C", Oxid. Met., Vol. 84, No. 5, 2015, pp. 567-584.
[21] K. Hay, F. Hicks, D. Holmes, "The transport properties and defect structure of the oxide (Fe, Cr) 2O3 formed on Fe- Cr alloys", Materials and Corrosion, Vol. 21, No. 11, 1970, pp. 917-924.
[22] J. Pettersson, H. Asteman, J.-E. Svensson, L.-G. Johansson, "KCl induced corrosion of a 304-type austenitic stainless steel at 600 C; the role of potassium", Oxid. Met., Vol. 64, No. 1, 2005, pp. 23-41.
[23] E. Sadeghimeresht, L. Reddy, T. Hussain, N. Markocsan, S. Joshi, "Chlorine-induced high temperature corrosion of HVAF-sprayed Ni-based alumina and chromia forming coatings", Corros. Sci., Vol. 132, No. 2018, pp. 170-184.
[24] S. Karlsson, J. Pettersson, L.-G. Johansson, J.-E. Svensson, "Alkali induced high temperature corrosion of stainless steel: The influence of NaCl, KCl and CaCl2", Oxid. Met., Vol. 78, No. 1, 2012, pp. 83-102.
[25] K. Segerdahl, J. Pettersson, J.E. Svensson, L.G. Johansson, "Is KCl (g) corrosive at temperatures above its dew point? Influence of KCl (g) on initial stages of the high temperature corrosion of 11% Cr steel at 600° C", Proc. Materials science forum, 2004, pp. 109-116.
[26] M. Schütze, Protective oxide scales and their breakdown, ed., The Institute of Corrosion and Wiley Series on Corrosion and Protection, Sussex, UK, 1991,
[27] Y. Xie, J. Zhang, D.J. Young, W. Zheng, "Effect of Fe on corrosion of Ni-20cr and Ni-30cr alloys in wet CO2 gas at 650 and 700° C", Corros. Sci., Vol. 154, No. 2019, pp. 129-143.
[28] J. Askill, "Tracer diffusion in the chromium–nickel system", physica status solidi (a), Vol. 8, No. 2, 1971, pp. 587-596.
[29] J.-W. Park, C.J. Altstetter, "The diffusion and solubility of oxygen in solid nickel", Metallurgical Transactions A, Vol. 18, No. 1, 1987, pp. 43-50.
[30] D. Pruthi, M. Anand, R. Agarwala, "Diffusion of chromium in inconel-600", J.Nucl. Mater., Vol. 64, No. 1-2, 1977, pp. 206-210.
[31] R. Bender, M. Schütze, "The role of alloying elements in commercial alloys for corrosion resistance in oxidizing-chloridizing atmospheres. Part i: Literature evaluation and thermodynamic calculations on phase stabilities", Materials and Corrosion, Vol. 54, No. 8, 2003, pp. 567-586.
[32] B. Li, B. Gleeson, "Effects of silicon on the oxidation behavior of Ni-base chromia-forming alloys", Oxid. Met., Vol. 65, No. 1, 2006, pp. 101-122.
[33] H.P. Nielsen, F. Frandsen, K. Dam-Johansen, L. Baxter, "The implications of chlorine-associated corrosion on the operation of biomass-fired boilers", Progress in energy and combustion science, Vol. 26, No. 3, 2000, pp. 283-298.
[34] J.R. Nicholls, D.J. Hall, P.F. Tortorelli, "Hardness and modulus measurements on oxide scales", Materials at High Temperatures, Vol. 12, No. 2-3, 1994, pp. 141-150.